UCRL-91699
PREPRINT

PHOTOELECTRONIC TRAJECTORY ANATOMY OF RCA-C-73435 IMAGE CONVERTER AND ITS PERFORMANCE

C. C. Lai
L. B. Olk
R. D. Lear

This paper was prepared for submittal to the
IEE Conference on Photoelectronic Imaging
Savoy Place, London, England
September 10-11, 1985

June 7, 1985

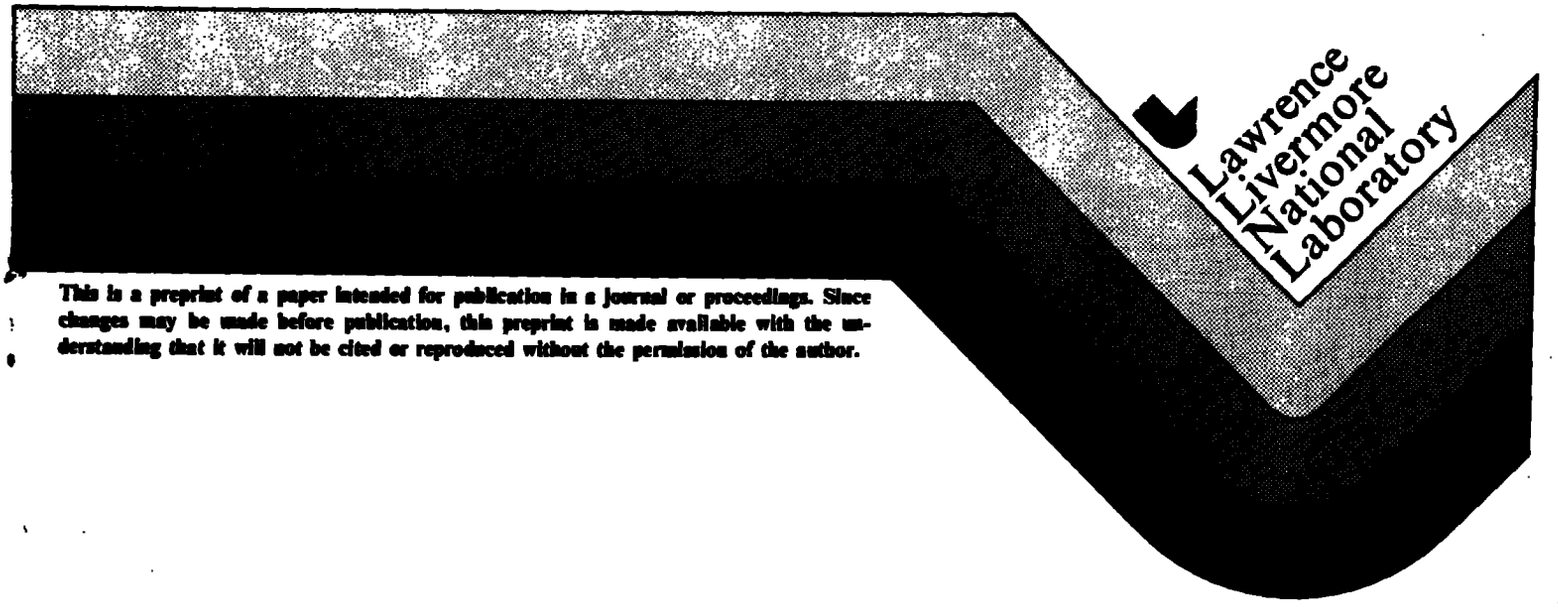

ABSTRACT

A two-dimensional electron-optics code, which fully incorporates space-charge and self-magnetic effects, was used to compute the photoelectronic trajectories in a RCA-C73435 image-converter streak tube. The code reveals the beam-trace formations in graphic detail as well as provides numerical data on static and dynamic imaging parameters, including focused-field profile, spatial resolution, linear distortion, transit-time dispersion and chromatic aberration. These computational results correlate qualitatively with the experimental ones obtained under corresponding conditions. The study thus establishes a set of computer-simulation estimates on tube performance as a function of the electron-emitting characteristics at the photocathode and as a function of the electrode voltages.

PHOTOELECTRONIC TRAJECTORY ANATOMY OF RCA-C73435 IMAGE CONVERTER AND ITS PERFORMANCE*

C. C. Lai, L. B. Olk and R. D. Lear

University of California, Lawrence Livermore National Laboratory
P.O. Box 808, Livermore, CA 94550

INTRODUCTION

In modern streak-camera applications, we increasingly need to capture simultaneously a large number of correlated, transient signal channels for technical or economical reasons. In addition, the quest continues for ultrafast temporal resolution. A streak tube with a large-format photocathode is preferred as it allows a maximum number of resolvable streak traces with minimum interline cross talk. The RCA C-73435 image-converter tube, with a large 1.37-inch-diameter photocathode, is uniquely proficient for meeting this need. Indeed, it has been widely adopted since its inception more than two decades ago. Numerous published articles (1,2) on this tube are mostly on application aspects and few are on tube-design related matters. In the present paper, we describe the tube's intrinsic behavior as predicted by the photoelectronic trajectory analyses, obtained by executing a two-dimensional electron-optics code, as well as the comparison with performance data obtained under corresponding conditions.

PHOTOELECTRON-TRAJECTORY CODE

For the analyses, we employed a modified code of W. B. Herrmannsfeldt's Electron Trajectory Program (3), GUNSLAC, in a CDC 7600 computer. This program code uses the finite-element method to solve the Poisson equation in two-dimensional cylindrical or rectangular coordinates. The code calculates the trajectory relativistically by a fourth-order Runge-Kutta method and accounts fully for both the electron-current-generated self-magnetic effect and the space-charge effect. This is achieved through proper charge deposition on each iteration cycle for recalculating both the Poisson equation and the trajectories until the solutions are converged. For each calculation, the code accepts a maximum total of 9001 active elements of square mesh within the allowable grid size of 100- by 300-mesh. However, a provision exists for focusing on any regional critical area for a separate precision calculation using a much finer mesh scale.
Input to the code consists of an electrode-boundary condition and an electron-launching state. The boundary condition is described by the location, shape, and voltage of each electrode. The launching state is specified by the initial photoelectronic emitting energy, angle, current, and location on photocathode surface for each selected trajectory beam to be traced. Output from the code gives the position and transit time of each beam as it arrives at the phosphor screen. The code also plots all the trajectories and selected equipotential lines, along with and within the tube-boundary profile.

TRAJECTORY ANALYSES AND RESULTS

For the boundary conditions of a RCA C73435 image-converter tube, the dimensions of all electrodes except the deflector plates were carefully measured and scaled proportionally from x-ray radiographs. The voltages, taken from manufacturer's test data, were 15,000 volts for the anode, 1550 volts for the focusing (G2) electrode, and 155 volts for the gating (G1) electrode. The open grid-wire portion of the gating electrode was substituted with a thin disk. Profiles of the rotationally symmetrical electrodes were depicted on the finite-element grid space by the radial (R) and axial (Z) cylindrical coordinates in mesh units, each unit denoting 0.05-inch of the actual size. Thus, one single beam, originating from a location R on photocathode surface and at an angle θ to the surface normal, represents all emissions from the circle defined by R and aiming at the same angle θ. If we assume a Lambertian, cosine-dependent angular distribution for the emissions from a single origin on the photocathode, the cone with a half-solid-angle of $\theta = 71.6$ degrees can be calculated to enclose 90% of all the photoemissions. Therefore, to represent a realistic case, we launched one central and two edge beams from every selected emission origin and with different angles, energies, and currents. The central beam is normal to the photocathode surface, has 0.2-eV initial energy, and contains the current of 0.01 microamperes/radian/radius, which is equivalent to 63 electrons per nanosecond for a 0.05-inch circumferential segment. The two edge beams are on the opposite sides of the normal, with $\theta = 71.6$ degree on RZ plane; each beam has 0.1-eV energy and one tenth of the central-beam current. The assumed energy and current levels are estimated as near the same order of magnitude as that of a typical streak-camera operation with nanosecond-range resolution.

General Trajectory Characteristics

Figure 1 is the typical computer-output plot, showing the upper half of tube structure, equipotential lines, and trajectories. Those trajectories crossing into the lower half of the tube appear as mirror images reflecting from the center line. The nine emission origins on the photocathode are spaced equally in the radial direction at R=0 and R=1+2n mesh units, with n=1 to n=8. This plot demonstrates these qualitative features: (i) the equipotential lines are almost concentrically distributed within the active region, (ii) the trajectories are rather straightforward except those of the edge beams near the photocathode, and (iii) the trajectories crossover points of the corresponding beams from all emission origins converge into a tiny spot near the anode-aperture entrance. In addition, the thin disk of the gating electrode coincides with the equipotential surface in free space, as evident by the lack of trajectory difference between runs with the disk included in the boundary condition and runs without. Hence, the aforementioned substitution of thin disk for grid-wire is validated, and the presence of grid-wire is not expected to induce severe microlensing effects or image distortion in its vicinity.

*Work performed under the auspices of the U.S. Department of Energy by Lawrence Livermore National Laboratory under Contract W-7405-Eng-48.

Focused-Field Profiles

On an enlargement of Figure 1, we clearly observe each set of the three trajectories from a common origin converging into a fine spot near the screen. The positional distribution of these spots defines the profile of photoelectronic focused field. Figure 2 contains five such profiles inside the tube, each at a different G1 voltage, with the screen center being located at the coordinate origin and the photocathode at the far right. The profiles exhibit (i) a parabolic curvature, showing nearly 0.8-inch axial coordinate change from the center to the edge at 0.5-inch radius, and (ii) a pronounced G1-voltage dependence for the focused-field location, which results in an approximately 0.1-inch axial displacement for every 10-volt variation. A similar characteristic was consistently observed in our operational experiences with the tube.

Linear Distortions

Here, the linear distortion at R is defined as the percentage ratio of the difference in the linear magnification of unit axial length between R=0 and R to the linear magnification at R=0. Computer numerical printout provides the data for axial position of all trajectories arriving at the screen. Figure 3 shows the calculated linear-distortion results based on the positions of all the central-beam trajectories. It also includes the measurement results from a test-pattern image produced by another RCA C-73435 tube that provided all the test data presented in this paper. The difference between the two curves in Figure 3 is estimated to be within measurement uncertainties.

Spatial Resolutions

On the screen, the trajectory separation between the two edge beams from a common origin defines the image spot size within which we estimate 90% of the photoemission to be included. Thus for the analyses, the inverse of twice the separation in millimeters gives the spatial resolution in line pairs per millimeter with an estimated contrast modulation ratio close to 90%.

Figure 4 shows the calculated results, in which those near the center exceeds 50 line pairs per millimeter. Also shown are the visual-inspection results of a resolution test-pattern image, for which the subjective visual-limiting contrast ratio is only about 5%. Because of the lower contrast level, the test data are expected to be higher than the trajectory results, as indicated by the low-resolution data in Figure 4. The measured results near the center are greater than the upper resolution limit of the test pattern, 22.5 line pairs per millimeter. Note that the resolution measurement from the image on film can vary significantly with many factors (such as nonuniform responsivity, imperfect proximity focusing, input intensity nonuniformity, and others), whereas none of these are relevant to the trajectory computation. The hump in the test-data curve could be due in part to some of these factors.

Transit-Time Dispersions

The numerical printout provides the transit time for electronic propagation from photocathode to screen for each trajectory. Figure 5 shows the transit-time data for both the central and the edge beams as a function of the radial position at photocathode. The 60-picosecond difference between the central and the edge beams, which remains almost unchanged with location, represents the transit dispersion among the photoelectrons from one emission origin, thus, causing temporal spreading in streak traces. In contrast, the increase in transit time with radial position would merely appear as an increase in trace delay with the slit length toward the border in streak imaging.

Chromatic Aberrations

The initial energy of photoelectrons can affect the trajectories to an extent that significant image aberrations are produced. Physically, the maximum initial energy can be equated to the difference between the incident photon energy and the energy at the cutoff wavelength of the photocathode spectral response at the long wavelength limit. We assume 920 nm (equivalent to 1.35 eV) for the cutoff wavelength of the S20R photocathode with extended-red response, and we performed trajectory analyses for the initial energies covering the incident-light spectrum from 375 to 800 nm.

Figure 6 shows the transit-time dispersion rising from 60 picoseconds at 0.1-eV to 170 picoseconds at 1.86-eV. Figure 7 illustrates the trajectory-resolution degradation over the same initial energy range. One set of resolution data from the experiments using line-filtered monochromatic light are also plotted (see Fig. 7) versus the correspondingly decreasing nonlinear wavelength scale. To ensure consistent optical focusing, the input lens system was refocused prior to using each new line filter. Because of the contrast-ratio difference noted in the spatial-resolution section, the test data are expected to be higher than the trajectory results. However, a monochromatic incident light generates a group of photoelectrons having distributed energies; whereas, the trajectory analyses are based only on the photoelectrons having the maximum energy of the group. For this reason, each test datum in Fig. 7 should be compared with a trajectory resolution that is somewhat higher than the one beneath it.

CONCLUSIONS

The trajectory analysis illustrates for the first time the theoretical characteristics of the RCA C-73435 tube as governed by the electron-optics code. Some of the trajectory results are particularly valuable as they can not be measured accurately through experimental means. The trajectory code proves reliable for comparing with test data. With this study we have achieved better understanding of the tube and its performance.

REFERENCES

1. Schelev, M. Ya., Richardson, M. C., and Alcock, A. J., 1972, Rev. Sci. Instrum., 43, 1819.

2. Stoudenheimer, R. G., 1971, RCA Application Note AN-4789.

3. Herrmannsfeldt, W. B., 1979, SLAC-Report-226.

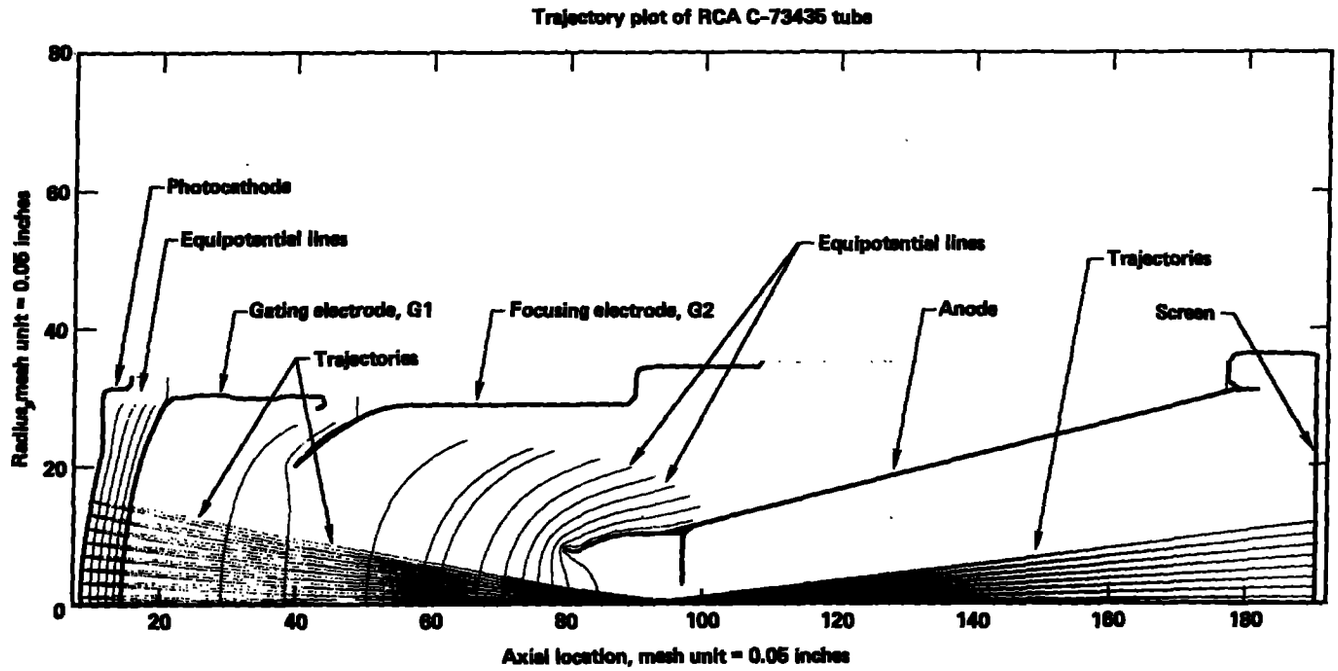

Figure 1. Photoelectronic trajectory plot of RCA C-73435 tube.

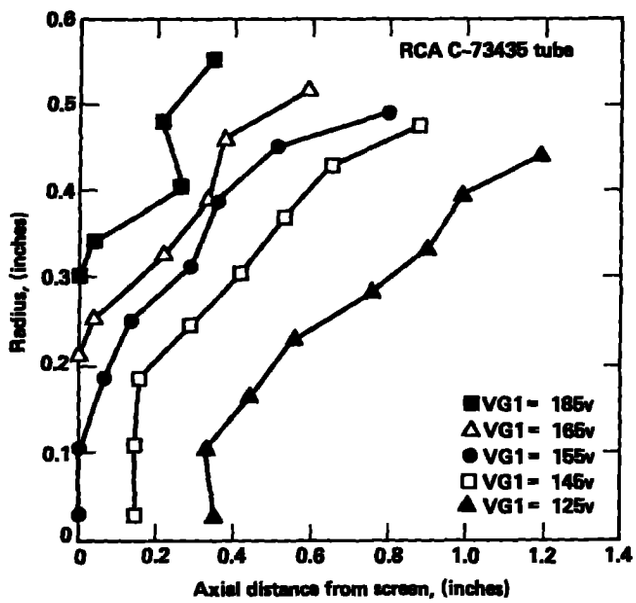

Figure 2. Focused-field profiles with the tube screen at x=0 axis and the photocathode at far right.

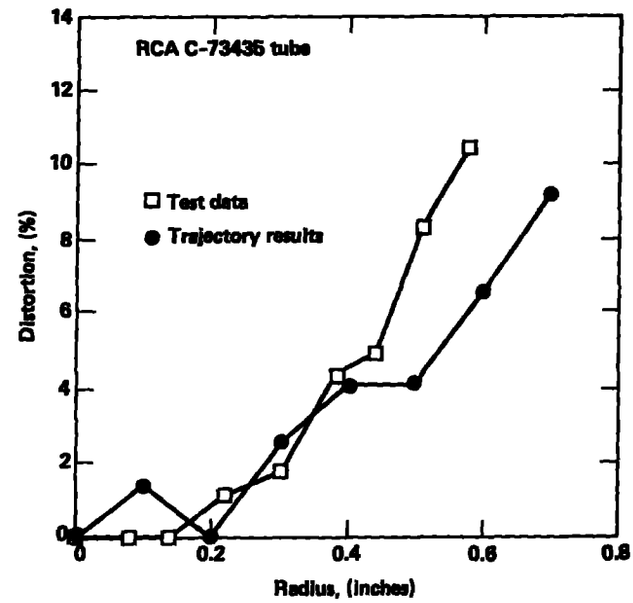

Figure 3. Linear distortions as a function of the radial position on screen.

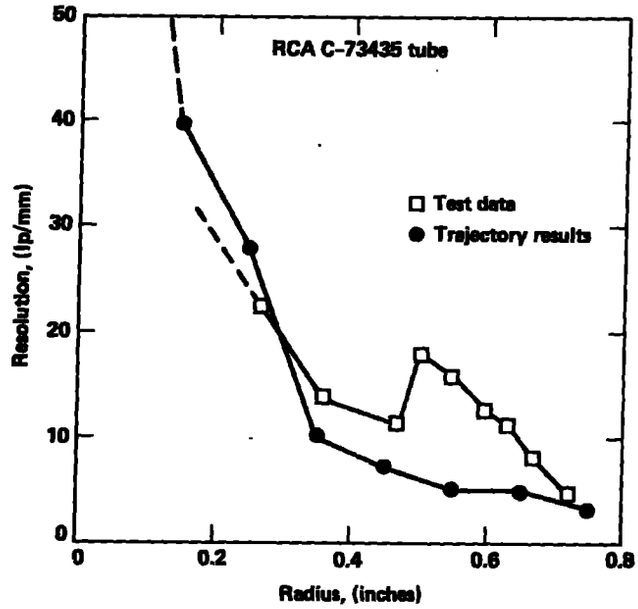

Figure 4. Spatial distortions as a function of the radial position on screen.

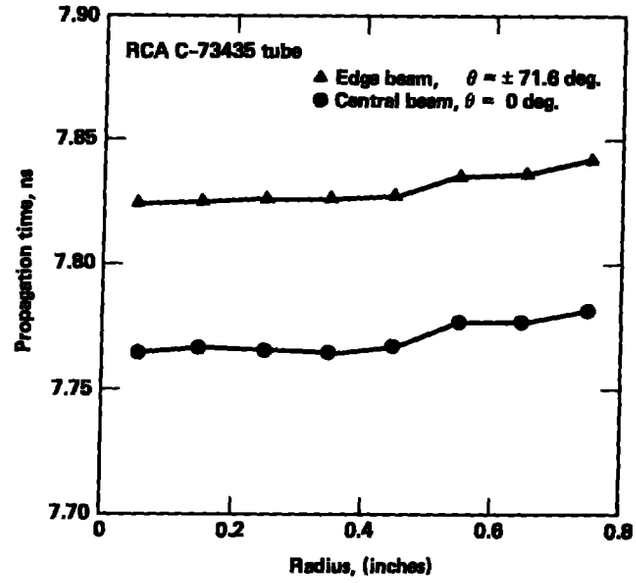

Figure 5. Transit time dispersions versus the radial position on photocathode.

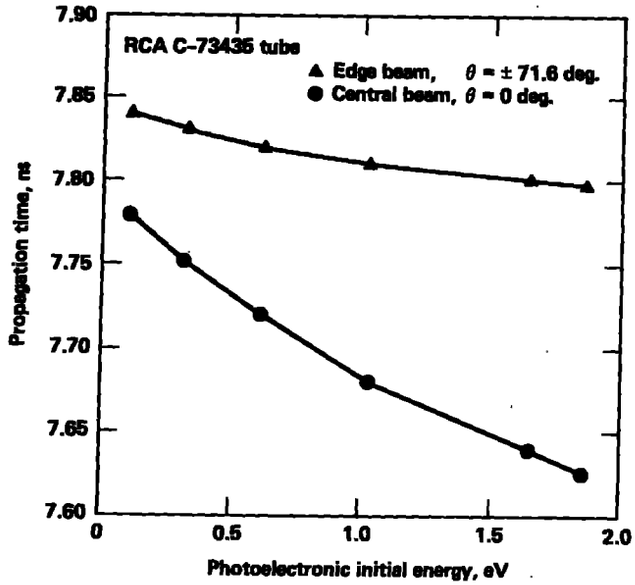

Figure 6. Chromatic aberrations in transit time versus photoelectronic initial energy.

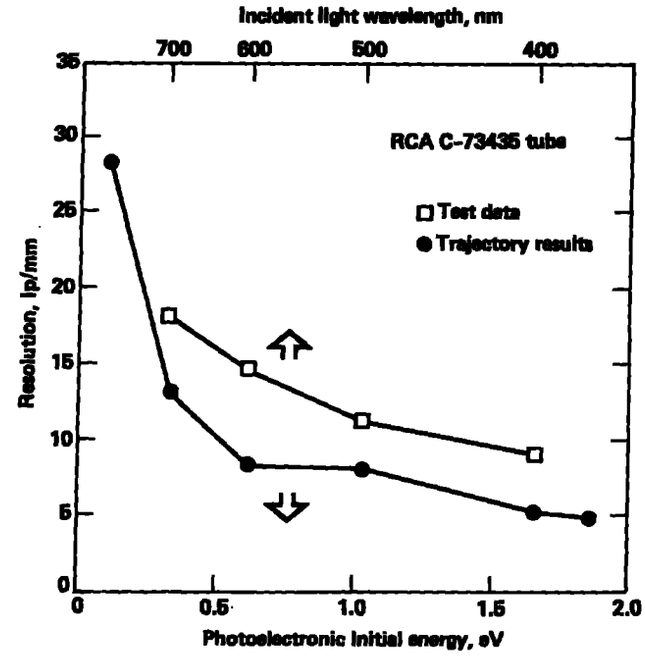

Figure 7. Chromatic aberrations in spatial resolution versus photoelectronic initial energy and incident-light wavelength.